Measurements of fireball onset

Brett Scheiner,[1,a)] Edward V. Barnat,[2,b)] Scott D. Baalrud,[1] Matthew M. Hopkins,[2] and Benjamin T. Yee[2]
[1]*Department of Physics and Astronomy, University of Iowa, Iowa City, Iowa 52240, USA*
[2]*Sandia National Laboratories, Albuquerque, New Mexico 87185, USA*

(Received 24 February 2018; accepted 19 March 2018; published online 12 April 2018)

Laser-based measurements of the characteristic features of fireball onset and stabilization in response to a stepped voltage applied to an anode immersed in a low pressure (100 mTorr) helium afterglow are reported. These include spatial and temporal evolution of metastable species, electron density, and electric field magnitude as measured by planar laser induced fluorescence, laser-collision induced fluorescence, and laser-induced fluorescence-dip spectroscopy, respectively. These measurements are found to be in qualitative agreement with recent particle-in-cell simulations and theoretical models [Scheiner *et al.*, Phys. Plasmas **24**, 113520 (2017)]. The measurements validate the simulations and models in which fireball onset was predicted to follow from the trapping of electrons born from electron impact ionization within a potential well created by a buildup of ions in the sheath. The experimental measurements also demonstrate transient features following the onset that were not present in previous simulations. New simulation results are presented which demonstrate that these features are associated with the abruptness of the voltage step used to initiate fireball onset. An abrupt step in the anode bias causes rapid displacement of ions and an associated plasma potential response following the sheath and fireball expansion. *Published by AIP Publishing.*
https://doi.org/10.1063/1.5026869

I. INTRODUCTION

Fireballs[1] are a discharge phenomenon that occur near electrodes that are biased at least $\mathcal{E}_I/e$ above the plasma potential, where $\mathcal{E}_I$ is the electron impact ionization threshold energy.[2] Fireballs are typically characterized by a luminous, usually quasi-spherical, region attached to the electrode and are much larger than the sheath scale.[3,4] The luminous region is usually associated with a quasineutral plasma within the fireball that is separated from the bulk plasma by a double layer. If a steady state is permissible, the double layer electric field accelerates electrons to the energies that are required for the electron impact ionization rate to maintain the fireball by balancing the ion loss rate through the fireball surface,[5] although this steady state is not always attained, e.g., Ref. 6. Fireballs are just one of the several forms of sheath structure that are possible near positively biased electrodes[2] and are of interest due to their application in dust confinement,[7] plasma contactors,[8] as an ion source[9] including those which can be used in the fabrication of nanodots,[10] and as a platform to study plasma self organization[11] and nonlinear processes.[12] Fireballs also bare a resemblance to similar phenomena that occur near hollow cathode plasma sources[13,14] and may contribute to the understanding of their operation.

Fireballs have most commonly been studied in argon plasmas with neutral pressures of 0.1–10 mTorr,[6] although they have also been observed in mercury vapor, helium, and neon at similar pressures.[15,16] The duration of fireball onset is typically a few microseconds[3] and has been observed to be induced by either an increase in neutral pressure or electrode bias.[3,17] Measurements of the fireball to date have been perturbative, utilizing Langmuir or emissive probes to measure density and electric potential. These have often been observed to cause the fireball to shift or jump to a new position on the electrode,[17] which can inhibit a reliable measurement. Therefore, there is a need for non-perturbative measurements to determine the unperturbed fireball behavior.

This work presents the first measurements of the fireball using non-perturbative laser based optical diagnostics. Using laser collision induced fluorescence (LCIF)[18,19] and laser induced fluorescence dip spectroscopy (LIF-dip),[20,21] 2D planar measurements of the electric field, helium metastable density, plasma emission, and electron density were made throughout the duration of fireball onset and stabilization. These provide the first experimental measurements of the topography of the fireball electric field and electron density, features that are critical to understanding the fireball onset.

The measurements are compared with a recent theoretical model and particle-in-cell (PIC) simulations of fireball onset.[5] In this model, fireball onset is predicted to follow from a buildup of positive space charge near the electrode due to ions born from electron impact ionization of neutral atoms. The positive space charge forms a potential well for electrons just in front of the electrode surface. Electrons born from impact ionization within this well are trapped, leading to an increase in electron density and eventually to the formation of a quasineutral fireball plasma. The topographical features of the newly presented measurements are found to be in agreement with prior PIC simulations. Further simulations are compared with the measurements to help discern the cause of transient features observed in the experiment which were not present in prior simulations.

[a)]Now at Los Alamos National Laboratory, Los Alamos, New Mexico 87545, USA. brett.s.scheiner@gmail.com.
[b)]evbarna@sandia.gov

This paper is organized as follows: an overview of the plasma chamber utilized to generate and the methods utilized to interrogate the fireball are described in Sec. II. Next, key characteristics of the spatial and temporal evolution of both the fireball and surrounding host plasma in response to the stepped anode voltage are presented in Sec. III. Discussion of the results is made through comparisons between observations, simulation, and predicted fireball behavior described in Ref. 5 in Sec. IV. Finally, concluding remarks are made in Sec. V.

II. SETUP AND DIAGNOSTIC METHODS

Plasma was generated in a stainless-steel vacuum chamber like the one depicted in Fig. 1. The chamber was evacuated by a turbomolecular pump to a base pressure of less than 5×10^{-7} Torr. Helium was introduced into the chamber at a rate of ∼10 sccm while the turbopump was throttled to achieve a nominal operating pressure of 100 mTorr. The base chamber consisted of an eight-inch (200 mm) spherical square vacuum chamber (Kimball Physics - MCF800-SphSqG2E4C4). A 6″ (150 mm) long, 8″ conflat nipple (6″ or 150 mm ID) was placed on the top of the chamber and housed a 4″ (50 mm) diameter electrode, marked "plasma generating electrode" in Fig. 1, that was periodically biased positive to generate a plasma inside the grounded chamber. An electrode assembly consisting of a 6″ OD aluminum plate with a 0.55″ diameter insert (centered) was housed on the lower 8″ conflat flange. A 0.5″ diameter electrode filled the insert; this is labeled the "fireball generating electrode" in Fig. 1. The outer 6″ diameter plate was tied to ground via a 1 MΩ resistor and the potential across the resistor was monitored with a voltage monitor with a nominal input impedance of 10 MΩ and a capacitance of 10 pF. The fireball generating electrode was periodically biased positive to initiate and then terminate the fireball. Voltage on and current to the anode was measured by voltage monitors placed across the series resistor which was nominally 1 kΩ. A photomultiplier tube was used to monitor optical emission emanating from the plasma. An interference filter with a 10 nm bandpass centered on 706 nm, close to the 3^3S to 2^3P transition at 706.5 nm, limited light collected by the photomultiplier tube. Voltage waveforms were monitored and recorded with a 12 bit, 1 GHz digitizing oscilloscope (Lecroy 6100).

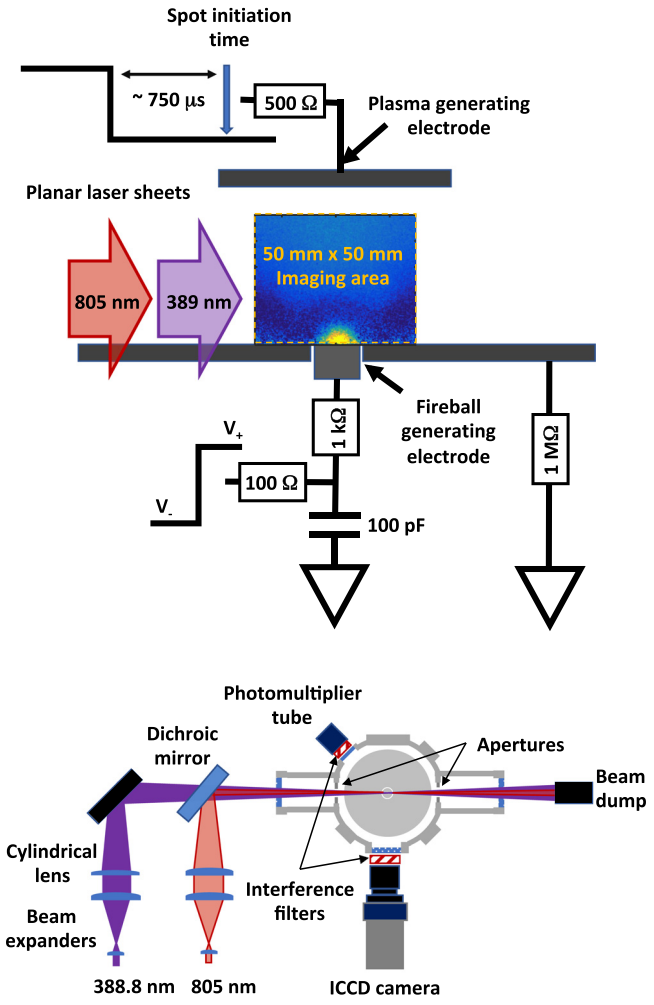

FIG. 1. Top: a side view schematic of the experiment setup showing the locations of the plasma generating electrode, the fireball generating electrode, and the imagining area. Bottom: a top down view showing the location of the diagnostic elements.

The biasing of both the plasma generating electrode and the fireball generating electrode was synchronized to the firing of the lasers at 20 Hz. Synchronization to the lasers and timing between the applied biases was achieved by a digital delay generator (SRS 645). Switching of both electrode potentials was performed by modified high voltage pulse generators (DEI, PVX-4150). The plasma generating electrode was biased at a 98% duty cycle and was biased on for 49 ms and then turned off (grounded) for 1 ms. The nominal operating voltage of the discharge power supply was +380 V, while the time averaged current was 100 mA. A 500 Ω series resistor was placed between the pulse generator and the plasma and served to stabilize the operation of the discharge, limiting the peak current to prevent a high current arc. The fireball was turned on ∼750 μs after the plasma generating electrode was turned off. The 750 μs delay between extinguishing the plasma generation process and fireball-initiation process allowed sufficient time for the plasma potential to relax to near ground potential as the electron temperatures cooled to sub-electronvolt levels. These features, while not directly observed, are consistent with the observed floating potential of the outer plate as it rapidly approaches ground potential and the extinguished optical emission as electron energies become insufficient to cause excitation. The fireball generating electrode was only biased on at 100 V for 20 μs of the 50 ms period. This short duration pulse was long enough to allow the fireball and host plasma to reach a steady state configuration while not long enough to modify initial densities of excited state species or charge species that could influence the initiation of subsequent fireballs.[22]

A. Diagnostic methods

The characteristics of the fireball formation and the resulting fireball structure were observed using both passive optical emission and active laser interrogation, as well as the current-voltage traces obtained through the setup described in Sec. II. Included in the methods categorized as active laser interrogation are planar laser-induced fluorescence (PLIF),[18] LCIF, and LIF-dip spectroscopy. While the aspects of these

diagnostics have been described elsewhere, an overview of specific details regarding how these methods were utilized and implemented in this study are discussed here. As illustrated in Fig. 2, all three methods are based on the same laser excitation pathway from a lower energy state to an intermediate state. The resulting laser-induced fluorescence generated after the laser excitation is the primary response that was monitored in these three methods. Differences in the methods depended on or utilized interactions of the laser excited state with energetic collisions (LCIF) or a second laser excitation to higher energetic states (LIF-Dip).

In this study, helium atoms in the 2^3S metastable state were interrogated with a 5 ns duration laser pulse tuned to the 2^3S to 3^3P transition at 388.8 nm. The laser pulse was generated by a tunable, narrowband ($<0.1\,cm^{-1}$) OPO laser system (Continuum Sunlite EX OPO) pumped by the third harmonic (355 nm) of a seeded, Q-switched Nd:YAG laser (Continuum Powerlite 9020) operating at 20 Hz. The output of the ~777.6 nm idler generated by the OPO was subsequently doubled (Continuum Sunlite FX) to generate ~2 mJ of 388.8 nm light used for laser excitation. The ~2 mm diameter 388.8 nm laser beam was expanded to a diameter of ~30 mm using a beam expander consisting of a pair of plano-convex lenses. After beam expansion, the collimated laser beam was focused into a planar sheet ~30 mm high and <1 mm wide by a 1000 mm focal length cylindrical lens.

Laser induced fluorescence was monitored by a gated, intensified CCD camera (Andor IStar) that was synchronized to the firing of the laser. The CCD consists of an array of 1024×1024 pixels and the imaged area was centered on the biased anode. The imaging area was 52 mm wide by 30 mm high, yielding an effective resolution of ~50 μm/pixel. Typical acquisition times were initiated 20 ns to 30 ns after the laser excites the interrogation volume and were 100 ns in duration. The 100 ns acquisition period results in LCIF signals that are integrated over the entire period. The LIF-dip measurements, on the other hand, represent the electric field values over the 10 ns laser pulse width. Narrow-band interference filters centered on transitions of interest, specifically emissions from the laser excited state (PLIF) and near-by states (LCIF), were utilized to suppress unwanted light emanating from other excited states.

As mentioned in the previous paragraph and illustrated in Fig. 2, laser induced fluorescence occurs at the same 388.8 nm frequency that was utilized in the excitation process. Because of this, considerable effort was taken to reduce the impact that stray or scattered laser light can have on the measurements. To mitigate this, the planar sheet of laser passed through angled windows as it was injected into and transported out of the vacuum chamber. Likewise, just prior to and after passing through the interrogation area where the fireball was formed, the laser sheet passes through two rectangular apertures that were 75 mm high and 5 mm wide to suppress back illumination of the interrogation volume from laser light scattered by the angled windows. Finally, the 2 mJ 388.8 nm laser beam was attenuated to levels ~250 μJ where LIF is sufficiently strong and backscatter is significantly reduced.

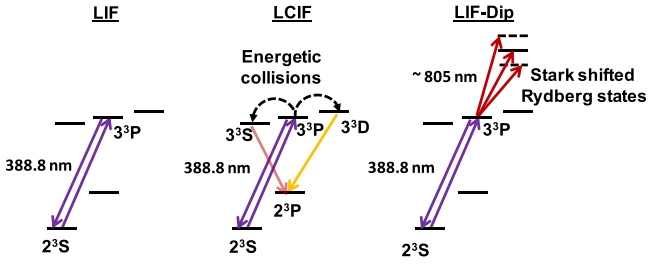

FIG. 2. An energy level diagram for transitions in helium that are used in the LIF, LCIF, and LIF-dip diagnostics.

1. Planar laser-induced fluorescence

When performing PLIF measurements of the spatial and temporal distribution of the helium metastable atoms in and around the fireball, two images are acquired. The first image consists of both laser induced fluorescence as well as the plasma induced emission generated at 388.8 nm. The second reference image consists of just the induced emission generated by the plasma. Both the total emission and plasma induced emission were acquired during the same period of time during the fireball formation process. For the acquisition of plasma emission, the firing of the laser was delayed by 200 ns to ensure image acquisition is complete prior to laser excitation. The laser-induced fluorescence was obtained by subtracting the reference emission from the total emission.

2. Laser-collision induced fluorescence

LCIF was utilized to measure the spatial and temporal evolution of electron density during fireball onset and stabilization. The implementation and execution of LCIF measurements were identical to that which was utilized for PLIF except that an extra set of measurements were made for emission from the nearby energetically uphill transition between 3^3D to 2^3P at 587 nm. For both of the observed transitions, both a total image (consisting of LIF or LCIF and plasma emission) and a reference image (plasma only emission) were acquired. As described in earlier studies,[18,21] an additional population of the 3^3D state occurs due to collisions between the laser excited 3^3P state and energetic plasma species such as electrons and neutrals. For the electron densities encountered in this study ($<10^{10}\,cm^{-3}$), the ratio of the LCIF from the 3^3D state to the LIF from the 3^3P state can be treated as linearly proportional to the electron density. At 100 mTorr, the contribution of energetic neutrals ($3.5 \times 10^{15}\,cm^{-3}$) produced an electron density independent contribution to the measured LCIF comparable to what would be generated by an electron density of $5 \times 10^8\,cm^{-3}$. This contribution, measured deep in the ion sheath (where electron density was orders of magnitude less than $5 \times 10^8\,cm^{-3}$), was subtracted from the total LCIF signals presented in this paper.

3. Laser induced fluorescence dip spectroscopy

LIF-dip spectroscopy was utilized to measure the electric field in and around the fireball. As described in earlier studies,[21] this method utilizes a second (probe) laser that excites a portion of the initial laser excited population produced by the

388.8 nm (pump) laser to Stark-shifted Rydberg levels as the probe laser is tuned across the transition. Detection of this shift provides a measure of the magnitude of the field, but not the field's direction. The probe laser was a second narrow-band OPO laser of the same make and specifications as the (pump) laser utilized to generate the PLIF at 388.8 nm. The firing of the probe laser was synchronized to the firing of the pump laser but was delayed by 15 ns. LIF at 388.8 nm was monitored as the probe laser was sequentially tuned across the targeted (Stark-shifted) Rydberg level. When the laser is in resonance with the transition there is a loss or depletion in the observed 388.8 nm LIF. As was done in both LIF and LCIF measurements, two images were taken per probe wavelengths. The first image (Total LIF) consists of both pump and probe lasers illuminating the interrogated volume, whereas the second image (Reference LIF) consists of just the pump laser. The LIF-dip signal is the difference between the Total LIF and Reference LIF images. Plasma induced emission was not explicitly accounted for as both images contain this information which gets subtracted out.

A mechanical shutter physically blocked the output of the probe laser while the Reference LIF images were being acquired. The coupling of the atomic orbitals of the helium atom to the external electric field causes a change in the energy eigenvalues of the orbitals and mixes the quantum states of differing angular momentum. The degree of mixing and induced energy shifts depends on both the magnitude of the electric field and the principle quantum number (n) of the atomic state probed. For the studies presented here, the $n = 28$ Rydberg state of helium was probed. Calibration of the spectral structure of Stark-shifted Rydberg states as a function of electric field was performed in a discharge chamber like the one described in an earlier study performed in argon.[21] The electric field sensitivity of the $n = 28$ Rydberg state was ~5 V/cm and was limited by the linewidth of the probe laser (~0.1–1 cm), while the maximum detectable field of 120 V/cm was limited by intermixing of the $n = 28$ state into nearby $n = 27$ and $n = 29$ states that smear the dip signal.

III. MEASUREMENTS OF FIREBALL ONSET

Measurements of fireball formation are presented in Figs. 3 and 4. The data presented in these figures represents an average over 1000 cycles of fireball formation. The stepped voltage was chosen to be from 55 V to 100 V, which was the smallest bias required to initiate a clearly developed fireball as defined by the presence of a region of electric field-free, quasi-neutral plasma separated from the bulk plasma by the strong electric field of a double layer. Observations include the applied voltage and the extracted current, as well as streak-like images (Fig. 3) that were formed by taking a time-stepped composite of axial profiles of the plasma induced emission measured at 590 nm ($3^3D \rightarrow 2^3P$), 2^3S metastable state measured by LIF, and electron density measured by LCIF. The axial profiles were centered on the axis of the anode and have been radially averaged over a ±1 mm window. Images were acquired over a 100 ns time window and were stepped at 100 ns intervals. Corresponding two-dimensional images of the

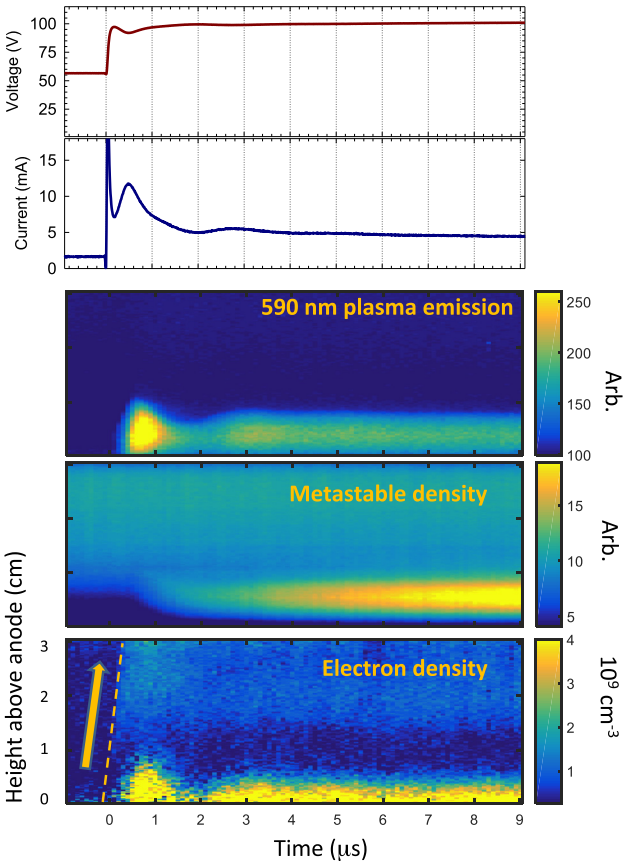

FIG. 3. Measured values of electrode bias, current collection, and plasma quantities. The plasma emission, metastable density, and electron density are plotted along a line perpendicular to the electrode as a function of time.

plasma induced emission at 590 nm, 2^3S metastable state, electron density, and the electric field measured by the LIF-dip are presented for selected times during the evolution of the fireball in Fig. 4. The imaged areas correspond to a 30 mm wide by 25 mm high area, centered about the anode.

Prior to the application of the voltage pulse there is evidence of an anode glow, which is a dimly glowing region that forms due to the electron-excited emission of neutral gas in the electron sheath.[23] In general, the formation of the fireball evolves in three stages. After the application of the voltage pulse, the first phase spans the initial 0.5 μs during which the fireball double layer structure is established. The second phase spans a period of time from 0.5 μs to 2 μs where transient fluctuations were observed. Finally, the third phase corresponds to the duration of time when the properties of the fireball change little in time.

A. Current and voltage trends

The applied voltage step and the resulting current collection are presented in the upper two plots of Fig. 3. Prior to the voltage step ($t = 0$), the current to the anode is ~1 mA and the anode voltage is ~55 V above chamber ground. When the bias transitions to 100 V at $t = 0$, there is a rapid surge in current drawn from the plasma. This surge is predominantly a displacement current (~20 mA) due to parasitic elements such as probe and chamber capacitance (~20 pF) in response to the rapid voltage change (~1×10^9 V/s). This is followed

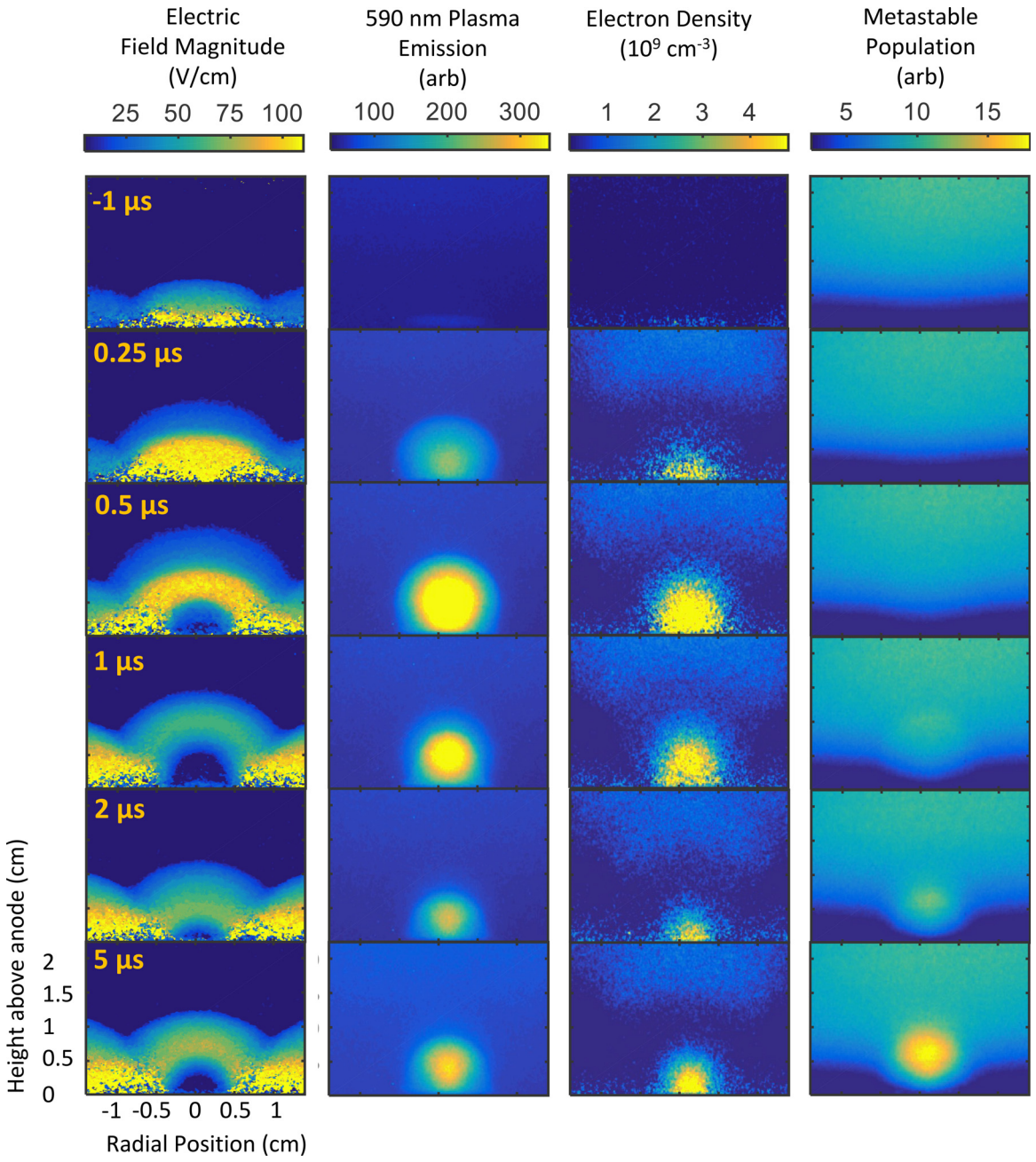

FIG. 4. 2D colormaps from experiments indicating the measured electric field, plasma emission, electron density, and metastable density before and after the voltage step was applied.

by a second slower surge in current that peaks at a value of 12 mA about ~0.5 μs after the application of the increase in electrode bias. This is a plasma based response and is not observed when the plasma in not present. The cause of this response is explored in the simulations presented in Sec. IV B. After the peak, the current subsequently decays and reaches a local minimum at ~2 μs and then is observed to fluctuate as the current slowly reaches a value of 4.9 mA, nearly 5 times the initial 1 mA draw.

B. Plasma emission

Prior to initiation of the voltage pulse, the plasma is essentially "dark" as it is anticipated that the effective electron energy or temperature has relaxed to levels below a point where significant optical emission can be generated. A faint glow extending ~2 mm above the anode is observable (Fig. 4) which is associated with excitation of neutrals due to electrons accelerated by the 55 V bias initially placed on the anode. Time resolved trends (Fig. 3) and snapshots (Fig. 4) of the optical emission during fireball onset indicate that a very bright region of excitation is formed in the immediate vicinity above the anode after the application of the voltage pulse at t = 0.

The first stage of the formation of this structure occurs over the first 0.5 μs of the applied pulse. At peak extension (t = 0.5 μs), the region of excitation extends ~10 to 12 mm from the anode while the radius of this excitation region roughly conforms to the radius of the anode. At the same time, it is observed that there is very little change in optical

emission emanating from the bulk plasma (far from the anode). The peak in emission and extension from the anode corresponds to the surge in current described in Sec. III A.

During the second stage of the fireball formation (~0.5 μs to 2 μs), the bright region is observed to contract while the intensity of emission becomes greatly reduced. At minimum extension, the region of excitation extends ~5 mm from the anode but still maintains its radial dimension, conforming to the radial extent of the biased anode. During this time, there is some increase in optical emission from the bulk plasma which starts farther from the anode and moves towards the anode (Fig. 3). This is consistent with a raised plasma potential and better confinement of energetic electrons from loss at the chamber wall sheath. A similar raise in plasma potential is seen during a similar fireball contraction observed in the simulations; see Sec. IV B. The second stage of the fireball formation process corresponds to the period of time where the current to the anode decays after the initial surge.

Finally, the third stage occurs after ~2 μs when the region of excitation begins to recover in both size and intensity, and extends to a distance of ~9 mm from the anode. It is likewise noted that there is little increase in the plasma emission from the bulk of the plasma. Furthermore, there is a faint but distinct dark region of reduced emission that spans a distance of ~12 mm to 18 mm that separates the bulk from the fireball. Little change of the region of excitation is observed for times later than 5 μs.

C. Metastable generation

In contrast to the measured current and optical emission, the metastable generation is a monotonic process in time and does not demonstrate an initial surge or relaxation. Prior to the stepped voltage, there is a residual population of metastable species that persists 750 μs after the plasma is extinguished. The concentration of metastable species is greater in the bulk and becomes reduced near the anode, likely due to losses to the wall. There is a slight augmentation in the metastable species in the region just above the anode which is likely due to the +55 V bias placed on the anode that leads to some excitation. During the first stage of fireball onset, almost no change in the metastable population is observed. On the other hand, during the second stage, there is some notable generation of metastable species that first peaks in a region spanning 8 mm to 10 mm from the anode and then moves towards the anode with time. By the third stage, most of the metastable generation occurs in a region spanning 5 to 8 mm above the anode. It is observed that the metastable species continues to be produced during the second and third phase.

D. Electron density

The temporal and spatial evolution of the electron densities have similar characteristics as the optical emission but with some notable differences. Prior to fireball onset, the measured electron density is $\sim 2 \times 10^8$ cm^{-3} which is comparable to the detectable limit at 100 mTorr. There is some augmentation of electron density in the 2 mm region above the anode but the degree is difficult to ascertain due to the limited signal that is generated in the immediate proximity of the surface. This augmentation is likely due to the 55 V bias placed on the anode and the presence of an anode glow. At the onset of the voltage step, a surge of electron density is observed not only in the near region of the anode but also in the bulk plasma. The electron densities near the anode exceed 5×10^9 cm^{-3} while the electron densities in the bulk are closer to 2×10^9 cm^{-3}. As hinted at in the optical emission, there is a region of lower electron density that connects the anode and the bulk plasma. This is caused by the rarefaction of the electron density in the strong electric field of the double layer.

From the time evolution of the electron density, it appears as if there is a wave or a front of electrons emanating from the anode and flowing into the bulk plasma. This expanding front is called out by the dashed line and arrow in Fig. 3 and is discussed alongside simulation results in Sec. IV B. During the second phase of fireball onset between 0.5 μs and 2 μs, the electron cloud established in front of the anode contracts and almost disappears at 2 μs. Little change in the bulk electron density is observed. Finally, the third phase of the fireball formation process shows a dense electron cloud that extends ~4 mm from the anode and has a radius less than that of the stepped anode. A peak electron density of 5×10^9 cm^{-3} is observed directly in front of the anode while the bulk electron densities remain near $\sim 2 \times 10^9$ cm^{-3}.

E. Electric field

Prior to application of the stepped voltage, the electric field above the anode is stronger than those above the adjacent plate that is grounded via the 1 MΩ resistor. The potential of the anode is +55 V whereas the outer plate is ~+1.3 V above the ground prior to fireball onset. As mentioned in Sec. II A 3, the LIF-dip method yields the magnitude but not the direction of the electric field. Integration[24] of the electric field from Fig. 4 above the outer electrode far from the anode yields a 15 V potential difference, indicating that the plasma potential prior to initiation of the stepped voltage is ~16 to 17 V above the ground. Likewise, integration of the electric field from the anode to the bulk plasma (where fields become undetectable) yields a potential difference of 38 V.

During the first phase of fireball formation, after the stepped bias is applied to the anode, there is a notable increase in the strength in the electric field above the anode but the field above the outer plate changes a little. At this time, the bulk has not yet had enough time to respond to the change in bias. Based on integration of the fields above the outer electrode at late times, the plasma potential becomes ~21 V, only a change of 5 V compared to the value prior to the application of the voltage step. The electric field at the outer electrode indicates that the response of the bulk plasma potential occurs about ~0.5–1 μs after the stepped bias. This suggests that the timescale for the plasma potential response is associated with the timescale for electron diffusion to the nearest non-anode boundary. In fact, the time for 1 eV electrons to diffuse to the adjacent wall by elastic neutral collisions with a 100 mTorr helium background is estimated to be 1 μs, a value which is consistent with measurements.

Figure 4 shows that the interface between the anode and bulk plasma extends at least 12 mm from the anode. As time progresses to 0.5 μs, the anode interface extends beyond 15 mm. Furthermore, there is a collapse in the electric field in the immediate vicinity of the anode while the peak in the electric field occurs in the region of 6 mm to 8 mm above the anode. This indicates the formation of a quasineutral fireball plasma. The strong electric field between this region and the bulk plasma indicates the presence of a non-neutral double layer. This electric field is responsible for the rarefaction of the electron density observed in the same region. The potential difference above the outer plate becomes ~40 V indicating that the bulk plasma is beginning to respond to the applied voltage.

During the second stage of fireball onset, the field-free region grows to its maximum extent at 1 μs. The plasma potential based on integration of the field above the outer electrode is ~80 V. By 2 μs the field free region in the fireball temporally vanishes as the anodic interface appears to collapse. At this time, the peak field is considerably weaker than during the first phase of fireball onset. At 2 μs, the field peaks at ~70 V/cm a distance of 4 mm to 5 mm above the anode. The plasma potential remains at ~80 V. This transient behavior is explored in the simulations described in Sec. IV B. Finally, as the fireball stabilizes at 5 μs, the re-establishment of a smaller field free region is observed in the immediate vicinity of the anode. The plasma potential of 80 V remains unchanged.

IV. COMPARISON OF THEORY AND SIMULATION

A. Observations of fireball onset

In a previous paper,[5] a model for fireball onset was formulated based on observations from PIC simulations, the results of which are reproduced in Fig. 5. The model described fireball onset as a consequence of the buildup of positive space-charge within the sheath due to electron impact ionization of neutral atoms by electrons accelerated in the sheath electric field. Initially, electrons born from ionization are quickly accelerated to the anode by the sheath electric field while ions are accelerated out of the sheath by the same field, but at a much slower rate due to their larger mass. Figure 5 shows that immediately after the increase in anode bias (40 V to 50 V in this case) the sheath ion density begins to increase without a corresponding increase in electron density, as expected. Once a sufficient amount of positive space-charge is present near the anode the potential profile develops a local maximum off the anode surface. This local maximum, corresponding to the zero electric field region in the panel marked $t = 1.5$ μs in Fig. 5, is a potential well for electrons. Low energy electrons born from ionization within this well are trapped, allowing the electron density to increase. This trapping eventually leads to the formation of a quasineutral region where $E \approx 0$ and $n_e \approx n_i$ between $t = 1.5$ μs and $t = 2$ μs. Once quasineutrality is established, the double layer is predicted to move in the lab frame if there is an imbalance in the Langmuir condition[5] ($n_e V_e = \sqrt{m_i/m_e} n_i V_i$ where V_e and V_i are the electron and ion flow velocities), a conservation law that is satisfied in the rest frame of a double layer due to the conservation of momentum, energy, and mass.[25] Such an imbalance is predicted to lead to the expansion of the fireball plasma when the double layer moves outward from the anode surface.

This process is evident in the measurements of plasma emission and electron density presented in Figs. 3 and 4 and discussed in Secs. III B and III D. In the first ~0.1 μs after the voltage step, Fig. 3 shows an increase in plasma emission immediately off of the electrode surface. This region is present prior to an increased electron density in the same region. This is consistent with the description above, the early time plasma emission is an indication of ionization since the energy for excitation is close to the energy required for electron impact ionization (~20 eV vs 24.5 eV). Ion space charge builds up in the sheath to form an electron-trapping potential before an indication of increased electron density.

This same general trend is seen in the simulation described in Ref. 5. Figure 5 shows the electron density, electric field, and ionization rate. The ionization rate was used as a proxy for plasma emission for comparing the simulation and experiment. Little ionization is seen in front of the electrode before the voltage step from 40 V to 50 V. An increase in electrode bias is followed by an increase in the ionization rate, although initially there is no increase in electron density. The ionization rate is expected to be an indication of plasma emission, since there are similar energy thresholds for these interactions. This is consistent with the suggestion that the increased plasma emission in front of the electrode is an indication of the buildup of ions near the electrode.

The electric field from the simulation, shown in Fig. 5, can also be compared with the experimental values presented in Fig. 4. The electric field geometry and magnitude during fireball onset between $t = 0$ μs and $t = 2$ μs qualitatively agree with that between $t = 0$ and $t = 1$ μs in the experimental measurements in Fig. 4, however, the difference in plasma parameters and neutral pressure slow down the onset since they modify the electron impact-ionization rate.

One discrepancy between the experiment and simulation is in the relative timing between the appearance of a double layer in the electric field structure and the increase in electron density. Experimental measurements of the electric field and electron density in the 2D maps of Fig. 4 show that there is an increase in electron density at the electrode surface before the electric field develops a potential well in front of the electrode. The existence of increased electron density at $t = 0.25$ μs in a location where the electric field magnitude is ~100 V/cm suggests there may be a mismatch in the plasma conditions between the time of measurement of the electric field and electron density[26] or that the double layer electric field forms rapidly within the 100 ns signal integration window for the electron density. If the rate of electron trapping in the fireball rapidly increases over the 100 ns integration, the density near the end of the integration window will dominate the image and may not be representative of the entire window. The timing of LIF-dip measurement of the electric field on the other hand is much more precise, only being limited by the 10 ns pulse width of the laser. Therefore, the electron density may be representative of conditions up to 90 ns after the electric field measurement, depending on the rate of increase in electron density.

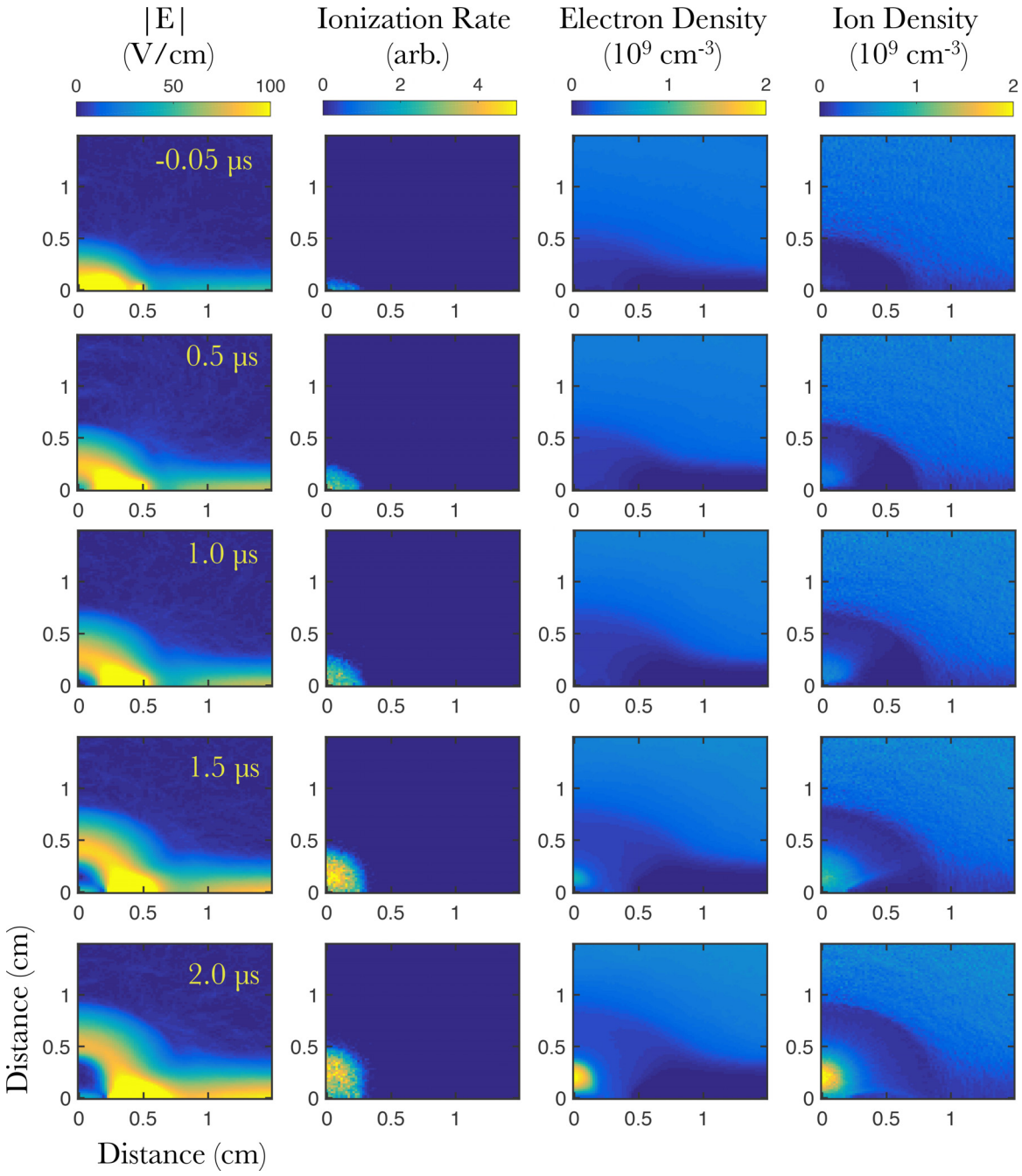

FIG. 5. 2D color maps of the simulated electric field magnitude, ionization rate, electron density, and ion density.

B. Transient behavior

A difference between the simulation and experiment setups was the values of the voltage step used to induce fireball onset. In the experiment, the increase in bias of the electrode was from 55 V to 100 V, while in simulation, this was from 40 V to 50 V. To understand the role of the voltage step in the transient behavior before fireball stabilization, two additional simulations were carried out.

Both simulations utilized the same setup described in Ref. 5, the only difference being the time dependent electrode bias. The goal of these simulations was to determine the role of the size and rate of different voltage steps. Both simulations utilized a step from 0 V to 120 V to induce fireball onset. The first simulation had the bias increased linearly over 0.6 μs resulting in a bias rate of 2×10^8 V/s, the same rate as the simulation in Ref. 5. The second simulation did the same over 1 ns resulting in a bias rate of 1.2×10^{11} V/s. The ion density, electric field magnitude, and plasma potential for each simulation are presented in the streak plots of Fig. 6.

For the simulation with the slower voltage step, shortly after the formation of the fireball, the electric field indicates that the inner edge of the double layer retracts towards the electrode between $t = 0.7$ μs and $t = 1$ μs, similar to the observation of transient fluctuations during fireball onset in the experiment. The retraction of the double layer surface coincides with a decrease in the ion density within the fireball.

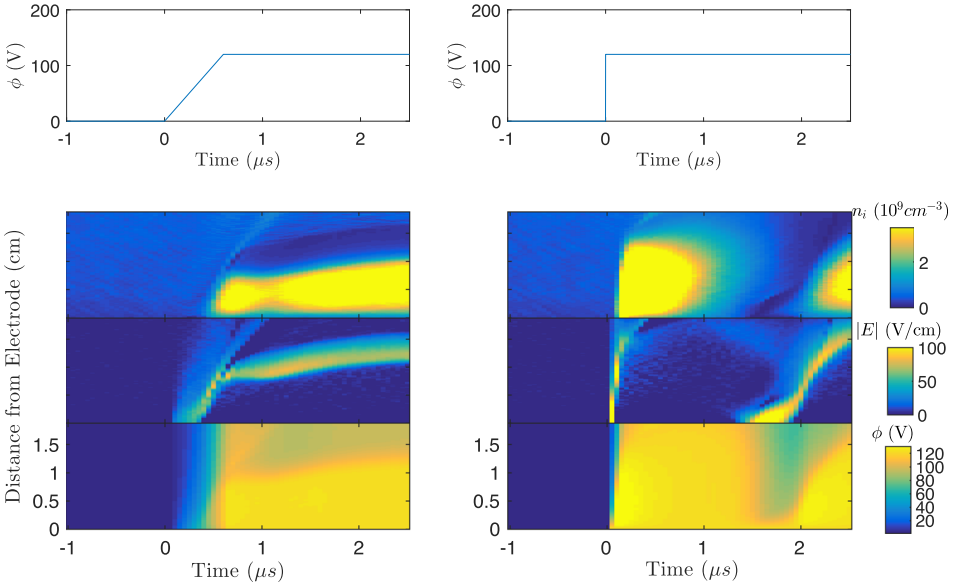

FIG. 6. PIC simulations of fireball formation with a voltage step from 0 V to 120 V shown in the top panels. The step duration in the left column is 0.6 μs and on the right is 1 ns. The ion density, electric field magnitude, and potential as a function of time are shown along a line perpendicular to the electrode.

The potential indicates that the fluctuation in the double layer position and ion density result from the response of the plasma potential to the displacement of bulk plasma ions by the rapid formation of the sheath and double layer electric field. The displaced ions ballistically respond to the electric field and are pushed out into the bulk plasma. This can be seen in both the ion density and electric field traveling along with the displaced ions. A similar feature is also seen in the measurement of the electron density in the experiment (Fig. 3). This is likely due to electrons being dragged along by the ion density disturbance. Similar to the experiments, the density disturbance is proceeded by the recession of the double layer surface. The simulation shows that once the ion density disturbance passes into the bulk plasma, the plasma potential peaks and then decays back to a steady value. It is this peak that decreases the energy of electrons crossing the electric field resulting in a temporary decrease in the electron impact ionization rate and ion density. Once a lower steady value of the plasma potential is reached, the electron impact ionization rate is restored and the double layer surface rebounds.

The simulation with the fast voltage step shows the effect of a more abrupt onset. The fireball quickly forms and the plasma potential quickly rises in the bulk plasma as the double layer quickly launches away from the electrode (near-vertical bright region near 0 μs in the electric field of Fig. 6). The increased plasma potential decreases the electric field of the double layer, which by t = 0.5 μs is only composed of a few volt difference from the bulk plasma. This decreases the energy of bulk electrons entering the fireball. The faster response of the plasma potential is caused by a larger displacement of ions due to the fast bias rate. In this case, there is little time for the local plasma potential to begin to respond prior to the ion density disturbance entering the bulk plasma, which can be seen at the top of the ion density plot in Fig. 6. Immediately after the plasma potential's rapid increase, ionization within the fireball ceases causing its collapse around 1 μs. This is followed by a much slower reformation of the fireball beginning at approximately 2 μs.

A comparison of the slow voltage step simulation with the simulation of Ref. 5 shows that the magnitude of the step also influences the transient behavior observed during spot onset. In both cases, the bias rate is 2×10^8 V/s, however, only the simulation with the 120 V step exhibits the transient behavior. This indicates that that the greater number of ions that are displaced the more susceptible the system is to exhibiting transient behavior. In this case, the larger voltage step results in a larger initial increase in the sheath area. The fast bias simulation indicates that the rate of the electrode bias is also important. If the bias changes so quickly that there is no time for the plasma potential to begin to respond before the ion density disturbance enters the bulk plasma the fireball fluctuations will be more dramatic, sometimes resulting in the complete collapse of the fireball. These simulations suggest the transient behavior will be minimized in cases with either smaller or slower voltage steps.

V. SUMMARY

This paper presents the first non-perturbative time resolved optical measurements of the fireball electric field magnitude and electron density during the fireball formation. The observations also represent the first experimental measurements of any kind to measure the 2D topographical features of the fireball electric field and electron density. LCIF measurements of electron densities and LIF-dip measurements of the electric field magnitude exhibit good agreement with recent PIC simulations of fireball onset.[5] The measurements of topographical features are found to be in close agreement with those presented in that reference as well. This validation of the model and simulations suggests that fireball onset results from the buildup of positive space charge and formation of a potential well that traps low energy electrons from electron-impact ionization, leading to a quasineutral fireball plasma.

The measured quantities also exhibited transient fluctuations during fireball onset, features which were absent in the previous PIC simulations. To better understand the cause of these fluctuations two new PIC simulations were run, varying the rate of the electrode bias. These simulations reproduced

the transient behavior seen in the experiment. Analysis of the simulations indicate that the transient behavior results from the displacement of ions from the expanding sheath and fireball electric field, an effect which is path dependent on the electrode bias. An ion density disturbance is driven ballistically into the bulk plasma causing fluctuations in the plasma potential which can shut off electron impact ionization within the fireball if large enough. Evidence for the ion density disturbance is seen in an experimentally measured electron density disturbance which likely results from electrons being dragged along by the positive space charge of the disturbance.

ACKNOWLEDGMENTS

This research was supported by the Office of Fusion Energy Science at the U.S. Department of Energy under Contract No. DE-AC04-94SL85000. The first author was also supported by the U.S. Department of Energy, Office of Science, Office of Workforce Development for Teachers and Scientists, and Office of Science Graduate Student Research (SCGSR) program. The SCGSR program is administered by the Oak Ridge Institute for Science and Education for the DOE under Contract No. DE-AC05-06OR23100.

[1]Fireballs are also commonly referred to as low pressure anode spots.
[2]I. Langmuir, Phys. Rev. **33**, 954 (1929).
[3]B. Song, N. D'Angelo, and R. L. Merlino, J. Phys. D: Appl. Phys. **24**, 1789 (1991).
[4]S. L. Cartier and R. L. Merlino, Phys. Fluids **30**, 2549 (1987).
[5]B. Scheiner, E. V. Barnat, S. D. Baalrud, M. M. Hopkins, and B. T. Yee, Phys. Plasmas **24**, 113520 (2017).
[6]R. L. Stenzel, C. Ionita, and R. Schrittwieser, Plasma Sources Sci. Technol. **17**, 035006 (2008).
[7]A. Barkan and R. L. Merlino, Phys. Plasmas **2**, 3261 (1995).
[8]E. Ahedo, Phys. Plasmas **3**, 3875 (1996).
[9]Y.-S. Park, Y. Lee, K.-J. Chung, and Y. S. Hwang, Rev. Sci. Instrum. **82**, 123303 (2011).
[10]S. Chauhan, T. Barman, M. Bhatnagar, M. Ranjan, and S. Mukherjee, Rev. Sci. Instrum. **88**, 063507 (2017).
[11]C. Maszl, J. Laimer, and H. Stori, IEEE Trans. Plasma Sci. **39**, 2118 (2011).
[12]R. L. Stenzel, J. Gruenwald, C. Ionita, and R. Schrittwieser, Plasma Sources Sci. Technol. **20**, 045017 (2011).
[13]B. R. Weatherford, E. V. Barnat, and J. E. Foster, Plasma Sources Sci. Technol. **21**, 055030 (2012).
[14]D. Levko, Phys. Plasmas **24**, 053514 (2017).
[15]D. Andersson, J. Phys. D: Appl. Phys. **14**, 1403 (1981).
[16]R. L. Stenzel, J. Gruenwald, C. Ionita, and R. Schrittwieser, Plasma Sources Sci. Technol. **21**, 015012 (2012).
[17]S. D. Baalrud, B. Longmier, and N. Hershkowitz, Plasma Sources Sci. Technol. **18**, 035002 (2009).
[18]E. V. Barnat and K. Frederickson, Plasma Sources Sci. Technol. **19**, 055015 (2010).
[19]E. V. Barnat and B. R. Weatherford, Plasma Sources Sci. Technol. **24**, 055024 (2015).
[20]U. Czarnetzki, D. Luggenhölscher, and H. F. Döbele, Phys. Rev. Lett. **81**, 4592 (1998).
[21]E. V. Barnat, Plasma Sources Sci. Technol. **20**, 053001 (2011).
[22]The time for helium species diffusion across the chamber is approximately 1 ms.
[23]The luminosity and size of the fireball is typically much greater than that of the anode glow.
[24]In this region, the electric field is integrated as a straight line perpendicular to the wall surface.
[25]B. Song, R. L. Merlino, and N. D'Angelo, Phys. Scr. **45**, 391 (1992).
[26]Note that the measurements were not simultaneous and that drifting plasma conditions can modify the timing of the onset. Care was taken to ensure that plasma conditions had stabilized before the measurement.